Research Square

Preprints are preliminary reports that have not undergone peer review.
They should not be considered conclusive, used to inform clinical practice,
or referenced by the media as validated information.

Closed-Form Storage Stability, Induction Delay, and Thermal- Feedback Criticality of Melt-Gated Autocatalytic Cure

Leon Sandler

sandler.leon@gmail.com

Independent researcher

Research Article

Keywords: autocatalytic cure kinetics, thermal runaway, encapsulated catalyst, reactor stability, Hopf bifurcation, hysteresis

Posted Date: November 3rd, 2026

DOI: https://doi.org/10.21203/rs.3.rs-11298219/v1

License: This work is licensed under a Creative Commons Attribution 4.0 International License.
Read Full License

Additional Declarations: No competing interests reported.

Closed-Form Storage Stability, Induction Delay, and Thermal-Feedback Criticality of Melt-Gated Autocatalytic Cure

Leon Sandler
Independent researcher, Northbrook, Illinois, USA
Corresponding author: sandler.leon@gmail.com
ORCID: 0009-0007-4584-808X

Abstract

We derive closed-form results for a lumped model of a cure triggered by the melting of an encapsulated catalyst, and test each against the full equations. At constant temperature the gated cure equals the ungated cure evaluated on the cumulative amount of catalyst released, so the gate delay grows with conversion and approaches the release time constant only late in the cure. The storage conversion of a Gaussian population of capsules follows from the fraction of capsules that are open, which bounds the spread of melting temperatures to within 3 % of the full equations. For a fully released catalyst, the thermal balance at fixed conversion has a critical value of the product of the reduced exothermicity and the ratio of thermal to reaction time, given in closed form (1.96 for reaction order 3/2); integrated thresholds approach it for fast heat loss, and Arrhenius kinetics raise it by about $\exp(1/Ar)$, with Ar the reduced activation energy (within 5 % on the tested grid). In a continuous-flow reactor with ungated kinetics, two folds of the steady-state curve do not imply two stable states: the upper branch can lose stability at a Hopf-type point before its fold. The window of two stable states is computed on an Arrhenius temperature path (24 K here), while sweep loops through that point depend on noise. All parameters are illustrative; no experimental data are used.

Article Highlights

- Melt-triggered catalyst release delays a cure by a conversion-dependent time, not a fixed one
- A closed-form rule limits the spread of capsule melting points for acceptable storage life
- In a flow reactor, two steady states must be checked for stability before predicting hysteresis

Keywords: autocatalytic cure kinetics; thermal runaway; encapsulated catalyst; reactor stability; Hopf bifurcation; hysteresis

1 Introduction

Encapsulating a reactive component and releasing it on demand is a general way to separate the stability of a formulation from the speed of its cure. The best-known instance is the self-healing polymer, in which embedded capsules release a healing agent when damaged [1]; thermally triggered variants use the melting of a wax or polymer shell, whose phase-change behavior is the subject of a literature on microencapsulated phase-change materials [2] and whose release is described by a family of release models [3]. When the released species catalyzes a thermoset

cure, three features interact: the capsule population has a distribution of melting temperatures rather than a single one, the cure is autocatalytic and follows the form introduced by Kamal and Sourour [4, 5], and the cure heat raises the temperature of the specimen, which accelerates the cure. The cure exotherm makes the temperature field of thick thermoset sections depend on the cure history [6], and the feedback between heat release and rate is the subject of the classical theory of thermal explosion of Semenov and Frank-Kamenetskii [7, 8]. That theory has been extended to reactant consumption [9] and to the induction period [10], and the multiplicity and stability of the steady states of a heated, continuously fed reactor were analyzed by van Heerden, by Aris and Amundson, and by Uppal, Ray and Poore [11–14].

Calorimetric kinetic analysis, usually by differential scanning calorimetry (DSC), is well codified [15, 16], and the separable form of the cure law is a standard route to closed-form cure times, with the temperature history entering through a generalized time [17]. In that literature the rate law and the thermal runaway of a specimen are usually treated separately. The question addressed here is narrower: for the lumped model of *a melt-gated* autocatalytic cure, which statements linking the quantities that a calorimeter measures (the rate constants of the cure, the width of the melting endotherm of the capsules, the thermal time constant of a specimen) to storage stability, delay and runaway can be written in closed form, and how well do they hold against the full equations?

The paper separates standard identities from results specific to this system. Proposition 1 is the generalized-time identity [17] applied to the catalyst availability; its content is the identification of the clock and the resulting delay law (Section 3.1). Proposition 2 collects standard integrals and one sharpness law (Section 3.2). Proposition 3, the storage conversion of a Gaussian capsule population and the bound on the melting-temperature spread that follows from it, is specific to the gated system (Section 3.3). Proposition 4 applies the Semenov fold of the frozen-conversion balance to the Kamal–Sourour consumption law, which gives a closed-form critical number, its overshoot below the fold and an Arrhenius correction (Section 3.4); the classical treatment of consumption [9] is not specific to autocatalysis. Proposition 5 gives the steady states, the Jacobian and the stable window of a continuous-flow reactor with this kinetics (Section 3.5). A synthetic-data test shows how the closed forms behave as fitting functions (Section 3.6). To the author's knowledge, in the sources examined, these results have not been assembled for a gated autocatalytic cure.

1.1 Relationship to previous computational work

The model equations of Section 2.1 (Eqs. (1)–(3)), the illustrative parameter set of Table 2, the capsule-population picture, the logistic activation and the reference integrator are those of an earlier numerical study by the author [18], posted as a ChemRxiv preprint and submitted for publication elsewhere; they are not claimed as new here. That study asks whether thermal gating improves delayed cure and answers it numerically (cure timing, comparison with first-order controls, gate-width trade-off, regime maps). A later version of the same numerical study [19] added numerical storage-stability and design-rule tables for capsule populations. Those numerical results are not presented as new here: Proposition 3 reproduces them from a closed form and uses them to test it. The present paper asks a different question: which statements about storage, delay, criticality and reactor stability can be derived analytically, and how well do they hold? Its own contributions are listed in Table 1. No figure of the earlier study is reproduced,

and its comparisons with first-order controls are not used. The related submission is disclosed to the editor in the cover letter. The model is lumped and every parameter is illustrative: nothing is fitted to measurements, and the paper makes no claim about a particular material.

Table 1 Provenance of the results: what follows from established theory and what is specific to this system (to the author's knowledge, in the sources examined).

Result	Established antecedent	Specific to the melt-gated autocatalytic system
Availability clock and delay (Prop. 1)	Generalized-time (time-change) identity of separable kinetics [17]	Identification of the clock with the integrated catalyst availability; the conversion-dependent delay $\tau_{rel}[1 - \exp(-t/\tau_{rel})]$; the clock for incomplete activation
Cure time and sharpness (Prop. 2)	Integrals of the Kamal–Sourour law [4, 5]	Exact $n = 1$ sharpness and its logarithmic asymptotic law (an elementary consequence)
Storage conversion and spread bound (Prop. 3)	Gaussian tail and probit approximation; linear response with an integrating factor	Closed-form storage conversion of a capsule population with release lag, and its inversion into a bound on the melting-temperature spread (exact within the Gaussian–logistic, small-conversion model)
Critical number (Prop. 4)	Semenov and Frank-Kamenetskii fold [7, 8]; reactant consumption [9]; induction period [10]	Closed-form maximum rate of the Kamal–Sourour law with an induction term, hence the finite-ε critical number; the frozen-fold Arrhenius factor; operational thresholds
Flow reactor (Prop. 5)	Multiplicity and stability of stirred reactors [11–13]	Closed-form equilibrium-multiplicity threshold κ_c for this kinetics; Jacobian and Hopf-type stable window; a temperature-path simulation with Arrhenius kinetics

2 Model and scaling

2.1 Equations

The conversion α of the resin obeys, in the rate equations (ordinary differential equations, ODEs) below, a Kamal–Sourour law with reaction order n for the unreacted fraction and first order in the autocatalytic term,

$$\frac{\mathrm{d}\alpha}{\mathrm{d}t} = \langle C\rangle(t)(k_1 + k_2\alpha)(1-\alpha)^n, \tag{1}$$

where $\langle C\rangle$ is the availability of the catalyst averaged over the capsule population (the fraction of the catalyst that has been released, $0 \le \langle C\rangle \le 1$). The temperature of the well-mixed specimen obeys a lumped energy balance with Newtonian loss and the adiabatic temperature rise ΔT_{ad} of the reaction,

$$\frac{dT}{\mathrm{d}t} = \frac{(T_\infty - T)}{\tau_{th}} + \Delta T_{ad}\frac{\mathrm{d}\alpha}{\mathrm{d}t}. \tag{2}$$

Capsule i has a melting temperature $T_{m,i}$, drawn from a Gaussian of mean T_m and standard deviation σ, and releases its catalyst by first-order relaxation toward a logistic activation of width w_0,

$$\frac{dC_i}{\mathrm{d}t} = k_{rel}(T)[G_i(T) - C_i], \quad G_i = \left(1 + \exp\left(-\frac{T - T_{m,i}}{w_0}\right)\right)^{-1}, \quad \langle C\rangle = \frac{1}{K}\sum C_i. \tag{3}$$

The initial state is $\alpha(0) = 0$ and $C_i(0) = 0$ unless stated, and $T(0) = T_\infty$ for the isothermal-start problems of Sections 3.1–3.4. The rate constants are Arrhenius, $k_j = A_j \exp(-E_j/RT)$, for $j = 1$ (background), 2 (autocatalytic) and rel (release). The model has no spatial structure, no diffusion control and no vitrification (Section 6). Throughout, the *illustrative* parameter set of Table 2 is used.

Table 2 Illustrative parameter set (not fitted to any material; taken from Ref. [18]). Arrhenius forms are $k = A \exp(-E/RT)$. Note that $E_1 \neq E_2$.

Quantity	Symbol	Value
Background rate constant	A_1, E_1	2.0×10^3 min^{-1}, 50 kJ mol^{-1}
Autocatalytic rate constant	A_2, E_2	2.5×10^7 min^{-1}, 65 kJ mol^{-1}
Reaction order	n	1.5 (1 and 2 where stated)
Release rate constant	A_{rel}, E_{rel}	6.4×10^6 min^{-1}, 60 kJ mol^{-1}
Mean melting temperature, activation width	T_m, w_0	118 °C, 0.5 °C
Adiabatic rise, thermal time constant	ΔT_{ad}, τ_{th}	220 K, varied (Section 3.4)
Rate constants at 140 °C	k_1, k_2, k_{rel}	9.53e-04, 0.151, 0.166 min^{-1}

2.2 Dimensionless groups and the exponential comparison model

Define $\varepsilon = k_1/k_2$, the thermal number $\Theta = \tau_{th} k_2(T_\infty)$, the reduced exothermicity $\psi = \Delta T_{ad} E_2/(RT_\infty^2)$, the activation number $Ar = E_2/(RT_\infty)$ and the release number $\Lambda = k_2/k_{rel}$. The combination that controls thermal feedback is

$$\Pi = \psi\Theta = \frac{\Delta T_{ad} E_2 \tau_{th} k_2}{RT_\infty^2}. \quad (4)$$

The *exponential comparison model* used in Sections 3.4 and 3.5 replaces the Arrhenius dependence of both rate constants by the common Frank-Kamenetskii (FK) form $k_j(T) = k_j(T_\infty) \exp(\psi\theta)$, $\theta = (T - T_\infty)/\Delta T_{ad}$, and treats ε as a constant. This is exact when the activation energies are equal and is a good description of the rate near the fold when the background term is negligible there: the fold occurs at conversions of order 0.4, where the autocatalytic term ($\alpha \approx 0.4$) exceeds the background term ($\varepsilon = 3 \times 10^{-3}$) by two orders of magnitude, so the different activation energy of k_1 (50 against 65 kJ mol^{-1}) matters little. The *Arrhenius simulations* of Section 3.4 (Table 6) do not use this simplification: both $k_1(T)$ and $k_2(T)$ follow their own Arrhenius law and $\varepsilon = k_1/k_2$ is evaluated at T_∞.

2.3 Computation and use of AI assistance

All numerical results are produced by the released scripts (run_all.py writes results.json; every number in the text is read from it, none is typed by hand), with the reference integrator, solver settings and protocols given in Appendix A. The model code, the closed-form module, the tests, the figure scripts and a first draft of the text were produced with the assistance of Claude Sonnet 5.5 (model identifier claude-sonnet-5-5; Anthropic), used through the Claude Code environment of the Claude desktop application on the author's computer (the model identifier is the one reported by that environment), because the author is an independent researcher without a computational group. The assistant wrote and ran code, drafted derivations and checked algebra; closed forms were verified against independent numerical integration by the test suite (code/test_theory.py) and by the comparisons reported in Section 3, and every journal reference was resolved through Crossref. The assistant did not enter or alter any numerical result by hand. The author is responsible for the content.

3 Results

3.1 Proposition 1: the gated cure runs on the clock of integrated availability

Proposition 1. At constant temperature, with $\alpha(0) = 0$ and $C_i(0) = 0$, let $F(\alpha) = (k_1 + k_2\alpha)(1 - \alpha)^n$. Then the gated conversion obeys

$$\int_0^{\alpha} \frac{\mathrm{d}x}{F(x)} = s(t), \;\; s(t) = \int_0^t \langle C \rangle(t')\mathrm{d}t'. \tag{5}$$

Proof. With T constant, $d\alpha/\mathrm{dt} = \langle C \rangle(t)F(\alpha)$ is separable: $d\alpha/F(\alpha) = \langle C \rangle \mathrm{dt}$. Integration from the initial state gives the identity. ■ This is the generalized-time identity [17] with the integrated availability as the clock. The left side is the isothermal time $t_{\mathrm{iso}}(\alpha)$ of the ungated resin, so the gated time to reach α is the time at which $s(t) = t_{\mathrm{iso}}(\alpha)$. For a population that is fully open at the operating temperature, $\langle C \rangle = 1 - \exp(-t/\tau_{\mathrm{rel}})$ with $\tau_{\mathrm{rel}} = 1/k_{\mathrm{rel}}$, so $s(t) = t - \tau_{\mathrm{rel}}[1 - \exp(-t/\tau_{\mathrm{rel}})]$ and

$$t_{\mathrm{gated}}(\alpha) - t_{\mathrm{iso}}(\alpha) = \tau_{\mathrm{rel}}\left(1 - \exp\left(-\frac{t_{\mathrm{gated}}(\alpha)}{\tau_{\mathrm{rel}}}\right)\right). \tag{6}$$

The delay is therefore conversion dependent: it lies between 0 and τ_{rel} and approaches τ_{rel} only when $t_{\mathrm{gated}} \gg \tau_{\mathrm{rel}}$. The fractional deficit from τ_{rel} is below 1 % when $t_{\mathrm{gated}}/\tau_{\mathrm{rel}}$ exceeds ln 100 = 4.605. At 140 °C (τ_{rel} = 6.02 min) the delay is 2.81 min at α = 0.001 ($t_{\mathrm{gated}}/\tau_{\mathrm{rel}}$ = 0.63), 5.12 min at α = 0.01, and 5.94, 6.02 and 6.02 min at α = 0.1, 0.5 and 0.9 (Table 3); the constant shift is a good description for $\alpha \gtrsim 0.1$ at this temperature and fails at early conversion. Independent adaptive integration of the gate and cure equations reproduces Eq. (6) to the integration tolerance in every row, and integrating the full model with the reference fourth-order Runge–Kutta (RK4) integrator at 125, 140 and 155 °C and α = 0.1, 0.5, 0.9 reproduces the gated times of Eq. (5) to a relative error of at most 7.7e-07.

For incomplete activation, with open fraction $f < 1$ (a fraction of the capsules that has not melted at the operating temperature), the clock is $s(t) = f[t - \tau_{\mathrm{rel}}(1 - \exp(-t/\tau_{\mathrm{rel}}))]$, so the delay relative to the ungated resin is not a constant shift: the gated cure is slowed in proportion to $1/f$ as well. For f = 0.5 at 140 °C the integrated times to α = 0.1, 0.5 and 0.9 are 45.1, 78.5 and 138.9 min, and the clock gives 45.1, 78.5 and 138.9 min, while the fully open population reaches them at 25.5, 42.3 and 72.4 min. A population whose mean melting temperature lies below the operating temperature is not necessarily fully open: a broad population has a tail of capsules that melt above it, and f must be computed from the melting-temperature distribution (Section 3.3). The statement is exact only at constant temperature; a heat-up transient or an exotherm adds a temperature-dependent delay that Proposition 1 does not describe.

Table 3 Delay of a fully open population relative to the ungated resin at 140 °C (n = 3/2, τ_{rel} = 6.02 min): integrated gate and cure equations against Eq. (6).

α	$t_{\mathrm{iso}}(\alpha)$ (min)	t_{gated} (min), integrated	Delay (min)	$\tau_{\mathrm{rel}}[1 - \exp(-t_{\mathrm{gated}}/\tau_{\mathrm{rel}})]$ (min)	$t_{\mathrm{gated}}/\tau_{\mathrm{rel}}$
0.001	0.97	3.78	2.81	2.81	0.63
0.01	6.32	11.45	5.12	5.12	1.90
0.1	19.55	25.49	5.94	5.94	4.23
0.5	36.24	42.26	6.02	6.02	7.01

α	$t_{iso}(\alpha)$ (min)	t_{gated} (min), integrated	Delay (min)	$\tau_{rel}[1 - \exp(-t_{gated}/\tau_{rel})]$ (min)	t_{gated}/τ_{rel}
0.9	66.42	72.45	6.02	6.02	12.03

3.2 Proposition 2: isothermal cure time, induction, and sharpness

Proposition 2. With $a = k_1$ and $b = k_2$, the isothermal time to reach conversion α is, for any n, $t_{iso}(\alpha) = \int_0^\alpha dx/[(a + bx)(1 - x)^n]$, and for $n = 1$

$$t_{iso}(\alpha) = \frac{1}{a+b} \ln \frac{a + b\alpha}{a(1-\alpha)}. \tag{7}$$

Proof. Partial fractions of $1/[(a + bx)(1 - x)]$ give $(a + b)^{-1}[b/(a + bx) + 1/(1 - x)]$, and integration gives the logarithm. ■ For small α the factor $(1 - x)^n$ is close to 1, so the induction time ($\alpha = 0.1$) is almost independent of n; the late-time tail is not. For $n = 1$ the sharpness $S = (t_{90} - t_{10})/t_{10}$ is exactly

$$S = \frac{\ln\left(\frac{9(a+0.9b)}{a+0.1b}\right)}{\ln\left(\frac{a+0.1b}{0.9a}\right)} \tag{8}$$

and, for $b \gg 9a$ and $n = 1$ only, it reduces to the asymptotic law

$$S \approx \frac{2 \ln 9}{\ln\left(\frac{b}{9a}\right)}. \tag{9}$$

Sharpness is then controlled by the rate-constant ratio alone, and only logarithmically. At 140 °C, $b/a = 159$ gives $S = 1.48$ exactly for $n = 1$ and 1.53 from Eq. (9), with a difference of 3.4 %; the law is accurate to 5 % across 110–155 °C for $n = 1$. A hundredfold increase of b/a, from 159 to 15,900, lowers the exact S from 1.48 to 0.59, a factor of 2.5. For $n \neq 1$ the law does not apply: at 140 °C the integrated sharpness rises from 1.48 ($n = 1$) to 2.40 ($n = 3/2$) because of the longer tail, and the quadrature should be used. The closed forms and the quadrature reproduce the integrated t_{10} and t_{90} for $T = 110$–155 °C and $n = 1$ and 3/2 to within 1.2e-07 (relative).

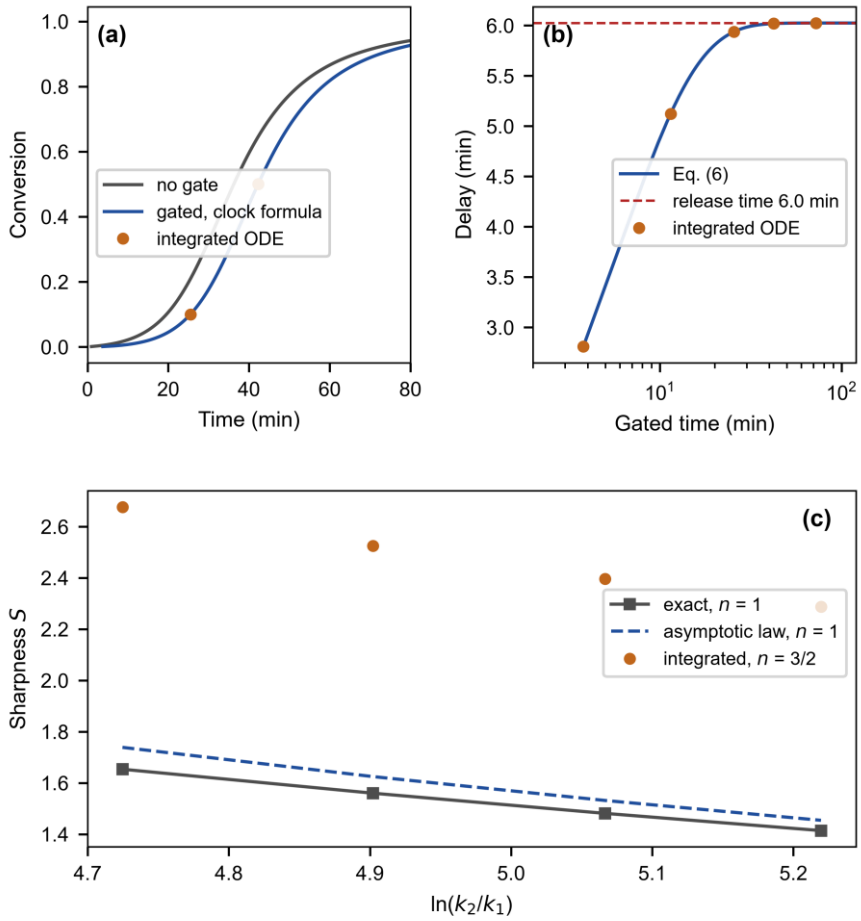


Fig. 1 (a) Gated and ungated cure at constant temperature (140 °C): the gated curve is the isothermal curve evaluated on the integrated-availability clock, and the integrated ODE (circles) agrees. (b) Delay of the gated cure relative to the ungated resin as a function of the conversion level: integrated (points), Eq. (6) (line), and the limit τ_{rel} (dashed). (c) Sharpness against the rate-constant ratio: exact $n = 1$, the asymptotic law Eq. (9), and integrated results for $n = 3/2$

3.3 Proposition 3: storage conversion of a capsule population and a bound on the spread

A capsule that is open at the storage temperature T_s releases catalyst that drives the cure at T_s. For a Gaussian spread σ of melting temperatures and a logistic activation of width w_0, the equilibrium open fraction at a margin $\Delta = T_m - T_s$ is the Gaussian–logistic convolution, which the probit approximation (matching the variance $\pi^2 w_0^2/3$ of the logistic) writes as

$$f = \Phi\left(-\frac{\Delta}{\sigma_{\text{eff}}}\right), \quad \sigma_{\text{eff}}{}^2 = \sigma^2 + \frac{\pi^2 w_0{}^2}{3}. \tag{10}$$

The approximation, not the identity, carries the error of this step; it is tested below. **Proposition 3.** If every capsule relaxes toward its own activation with the common rate constant $k_{rel}(T_s)$, then $\langle C\rangle(t) = f[1 - \exp(-k_{rel}t)]$ and, in the small-conversion limit ($\alpha \ll 1$, $(1-\alpha)^n \approx 1$), the storage conversion after a time t is

$$\alpha_s(t) = \frac{a}{b}[\exp(bf t_{\text{eff}}) - 1], \quad t_{\text{eff}} = t - \tau_{\text{rel}}\left(1 - \exp\left(-\frac{t}{\tau_{\text{rel}}}\right)\right). \tag{11}$$

Proof. In the small-conversion limit the rate law is linear, $d\alpha/\mathrm{d}t = \langle C\rangle(a + b\alpha)$, so that $\alpha = (a/b)[\exp(b\, s(t)) - 1]$ with $s(t) = \int\langle C\rangle \mathrm{d}t = f\, t_{\mathrm{eff}}$. ■ The tolerance η on the storage conversion (a symbol distinct from $\varepsilon = k_1/k_2$) then fixes the largest admissible open fraction, $f^* = \ln(1 + \eta b/a)/(b\, t_{\mathrm{eff}})$, which is exact for Eq. (10) as stated (that is, within the small-conversion linear response and the Gaussian–logistic description of the open fraction), and the bound on the spread follows by inverting Eq. (10), including w_0:

$$\sigma^* = \sqrt{\left[\left(\frac{\Delta}{z^*}\right)^2 - \frac{\pi^2 {w_0}^2}{3}\right]},\quad z^* = -\Phi^{-1}(f^*). \tag{12}$$

This is defined for $0 < f^* < 1/2$ (a finite positive bound). If $f^* \geq 1/2$ no finite upper bound on the spread is imposed, because even a population centered at the margin Δ above the storage temperature cannot exceed the tolerance; if the radicand is negative, even $\sigma = 0$ violates the tolerance because the logistic width alone opens too large a fraction. Eq. (12) with $w_0 = 0.5$ °C generated Table 4; the column for $w_0 \to 0$ shows the limit, which differs from it most for the narrowest widths. We tested the closed forms against the capsule-population equations ($K = 3201$ deterministic Gaussian quantiles of the melting temperature, constant temperature, $t = 150$ min; the discretization error of this population is at most 0.05 %, Appendix A, and is therefore not part of the quoted deviations) for margins of 3, 6 and 10 °C and spreads of 2–10 °C: the storage conversions agree within 5 % (difference = closed form/numerical − 1; median ratio 0.992), the closed form agrees with the defining integral to 4e-16, and the spread σ^* that solves $\alpha_s = \eta$ agrees with the root of the population equations within 3 % for all 8 cases in which the ODE reaches η (Table 4). For $\eta = 0.01$ and a 6 °C margin the bound is $\sigma^* = 5.9$ °C.

Table 4 Largest admissible melting-temperature spread σ^* for a storage time of 150 min and $w_0 = 0.5$ °C: Eq. (12), its $w_0 \to 0$ limit, and root-finding on the population equations (difference = closed form/ODE − 1).

Margin Δ (°C)	Tolerance η	f^*	σ^* Eq. (12) (°C)	σ^*, $w_0 \to 0$ (°C)	σ^* population ODE (°C)	Difference
3	0.001	0.019	1.13	1.45	1.12	+1.4 %
3	0.01	0.134	2.55	2.71	2.52	+1.1 %
3	0.05	0.331	6.79	6.85	6.59	+3.0 %
6	0.001	0.022	2.84	2.99	2.84	+0.1 %
6	0.01	0.156	5.87	5.94	5.85	+0.4 %
6	0.05	0.389	21.34	21.36	21.90	-2.5 %
10	0.001	0.027	5.12	5.20	5.12	+0.0 %
10	0.01	0.194	11.53	11.57	11.53	+0.0 %
10	0.05	0.489	> 40	> 40	> 40	–

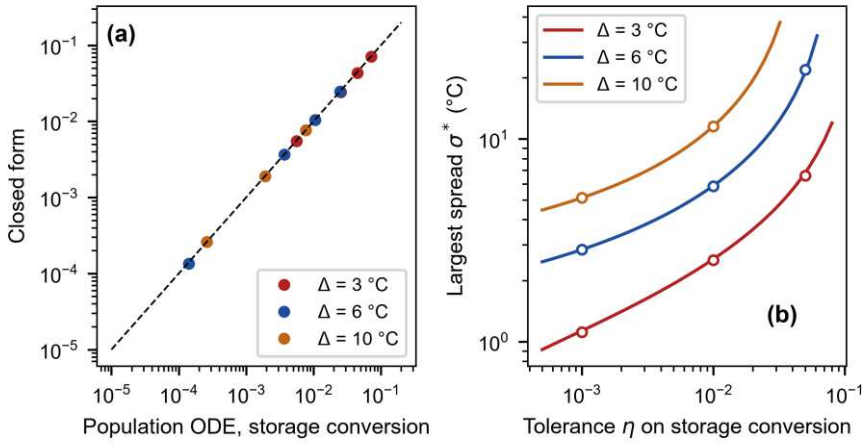


Fig. 2 (a) Closed-form storage conversion Eq. (11) against the population ODE for margins of 3, 6 and 10 °C. (b) Largest admissible spread σ^* (Eq. (12)) as a function of the tolerance η; open symbols are roots of the population ODE

3.4 Proposition 4: thermal-feedback criticality, overshoot, and Arrhenius correction

When the thermal time constant is short compared with the reaction time ($\Theta \ll 1$), the temperature rise $\theta = (T - T_\infty)/\Delta T_{ad}$ of the exponential comparison model follows the reaction quasi-statically with the conversion frozen, $\theta = \Theta\, r(\alpha) \exp(\psi\theta)$, where $r(\alpha) = (\varepsilon + \alpha)(1 - \alpha)^n$ is the isothermal rate in units of k_2. Multiplying by ψ gives $\psi\theta \exp(-\psi\theta) = \Pi r$, whose solution, if $\Pi r \le 1/e$, is

$$\psi\theta = -W_0\big(-\Pi r(\alpha)\big). \tag{13}$$

Proposition 4. For the ungated exponential model in the quasi-steady limit with frozen conversion, the low-temperature algebraic branch of Eq. (13) ceases to exist when $\Pi r(\alpha) = 1/e$. Maximizing r over α gives the limiting fold criterion. For $r = (\varepsilon + \alpha)(1 - \alpha)^n$ the interior maximum is at $\alpha^* = (1 - n\varepsilon)/(1 + n)$, provided $n\varepsilon < 1$, with $r_{max} = n^n(1 + \varepsilon)^{n+1}/(1 + n)^{n+1}$, so

$$\Pi_c = \frac{1}{e r_{max}} = \frac{(1+n)^{1+n}}{e n^n (1+\varepsilon)^{1+n}}, \quad \Pi_c \to e^{-1}\frac{(1+n)^{1+n}}{n^n} \quad (\varepsilon \to 0). \tag{14}$$

The finite-ε value is 1.4627, 1.9641 and 2.4610 for $n = 1$, 3/2 and 2 at $\varepsilon = 3 \times 10^{-3}$, against the $\varepsilon \to 0$ limits 1.4715, 1.9789 and 2.4832; the finite-ε formula explains why the integrated values of Table 5 at small Θ lie slightly below the limits. Below Π_c the quasi-steady peak is $\psi\theta_{peak} = -W_0(-\Pi/(e\Pi_c))$, and close to the fold it follows $\psi\theta_{peak} \approx 1 - [2(1 - \Pi/\Pi_c)]^{1/2}$, the normal form of a saddle-node bifurcation of the algebraic equation [20, 21]. This is a statement about the frozen-conversion algebraic manifold. For a finite batch the reactant is consumed and the temperature rise is bounded by the available reaction heat, so whether the fold marks ignition must be tested by integration. We therefore define an *operational* threshold as the Π (or ΔT_{ad}) at which the integrated peak rise exceeds $0.3\Delta T_{ad}$, and the conclusions about overshoot below are numerical. For comparison, the classical Semenov criterion for a source without consumption, $r = 1$ in the same units, gives $1/e = 0.37$; consumption and autocatalysis raise the frozen-conversion critical number by the factor $1/r_{max} \approx 5.4$ for $n = 3/2$ (reactant consumption in the Semenov problem was treated in Ref. [9]).

Verification in the exponential model. We integrated the exponential-form equations with isothermal start and bisected the operational threshold ($\varepsilon = 3 \times 10^{-3}$; Table 5). As $\Theta \to 0$ the operational Π_c converges to Eq. (14) with finite ε: at $\Theta = 0.003$ the values are 1.471, 1.974 and 2.472 against 1.463, 1.964 and 2.461 (differences 0.4–0.6 %). The threshold definition matters little (Π_c = 1.974, 1.974, 1.992 for 0.15, 0.3 and 0.6 of ΔT_{ad}). The finite-Θ shift is upward ($\Pi_c = 2.33$ at $\Theta = 0.1$ for $n = 3/2$); it is computed, not given in closed form. At $\Theta = 0.002$ the integrated peak at 0.5–0.98 Π_c follows the Lambert-W formula and approaches the square-root form (Fig. 3b).

Table 5 Critical thermal-feedback number in the exponential (Frank-Kamenetskii) model: operational thresholds from integrations (peak rise $0.3\Delta T_{ad}$, $\varepsilon = 3 \times 10^{-3}$) against Eq. (14) with finite ε and its $\varepsilon \to 0$ limit.

n	Θ	Π_c, integrated (operational)	Π_c, Eq. (14) finite ε	Π_c, $\varepsilon \to 0$
1.0	0.1	1.826	1.463	1.472
1.0	0.03	1.555	1.463	1.472
1.0	0.01	1.491	1.463	1.472
1.0	0.003	1.471	1.463	1.472
1.5	0.1	2.333	1.964	1.979
1.5	0.03	2.063	1.964	1.979
1.5	0.01	1.997	1.964	1.979
1.5	0.003	1.974	1.964	1.979
2.0	0.1	2.857	2.461	2.483
2.0	0.03	2.573	2.461	2.483
2.0	0.01	2.498	2.461	2.483
2.0	0.003	2.472	2.461	2.483

Arrhenius kinetics. For a single Arrhenius source at a temperature rise $x = \Delta T/T_\infty$ the exponent is $Ar{\cdot}x/(1 + x)$, against $Ar{\cdot}x$ in the exponential model. With $y = \psi\theta$ the frozen-conversion balance is $y \exp[-y/(1 + y/Ar)] = \Pi r$, and its fold is at y_f satisfying $y = (1 + y/Ar)^2$; the critical number is then

$$\Pi_c^{\mathrm{Arr}} = \Pi_c^{\mathrm{FK}} \cdot \mathrm{e}\, y_f \exp\left(-\frac{y_f}{1 + y_f/Ar}\right) \approx \Pi_c^{\mathrm{FK}} \exp\left(\frac{1}{Ar}\right) \tag{15}$$

The factor $\exp(1/Ar)$ is only the first-order (large-Ar) estimate of the first factor; for Ar = 18.0–19.9 the two differ by about 0.3 %. With distinct activation energies of the competing rate terms the fold condition must be solved for the actual sum of rates. We tested the correction with the true Arrhenius model (ungated, isothermal start, both k_1 and k_2 Arrhenius) at 120, 140 and 160 °C (Ar = 18.0–19.9) and Θ = 0.01, 0.03, 0.1, bisecting the adiabatic rise to the same operational threshold (Table 6). The prediction $\Pi_c^{FK}(\Theta)$ times the fold factor is within 5.0 % of the Arrhenius threshold in every one of the nine cases (times $\exp(1/Ar)$: within 5.4 %; the uncorrected exponential value is off by 6–11 %). This is empirical agreement over the tested grid; the correction has not been tested at small Ar or for other Θ. Release lag raised the operational threshold in the cases tested: at $\Theta = 0.03$ it increased Π_c from 2.174, 2.188 and 2.200 to 2.184, 2.199 and 2.212 at 120, 140 and 160 °C. No general inequality is claimed, because a smaller availability at the same conversion does not by itself show that the temperature histories compare.

Table 6 Operational critical number of the Arrhenius model (ungated, isothermal start; peak rise $0.3\Delta T_{ad}$) against the exponential-model value FK(Θ) multiplied by the frozen-fold factor of Eq. (15) and by $\exp(1/Ar)$ (difference = prediction/Arrhenius − 1), and the effect of a release lag.

T (°C)	Θ	Ar	Π_c Arrhenius	Π_c FK(Θ)	× fold factor	Difference	× exp(1/Ar)	Difference	Π_c, release lag

T (°C)	Θ	Ar	Π_c Arrhenius	Π_c FK(Θ)	× fold factor	Difference	× exp(1/Ar)	Difference	Π_c, release lag
120	0.01	19.9	2.093	1.973	2.080	-0.6 %	2.074	-0.9 %	–
120	0.03	19.9	2.174	2.039	2.150	-1.1 %	2.144	-1.4 %	2.184
120	0.1	19.9	2.545	2.308	2.433	-4.4 %	2.427	-4.6 %	–
140	0.01	18.9	2.106	1.980	2.094	-0.6 %	2.088	-0.9 %	–
140	0.03	18.9	2.188	2.047	2.165	-1.1 %	2.158	-1.4 %	2.199
140	0.1	18.9	2.566	2.316	2.449	-4.6 %	2.441	-4.9 %	–
160	0.01	18.0	2.117	1.986	2.106	-0.5 %	2.099	-0.8 %	–
160	0.03	18.0	2.200	2.053	2.177	-1.0 %	2.169	-1.4 %	2.212
160	0.1	18.0	2.586	2.322	2.462	-4.8 %	2.454	-5.1 %	–

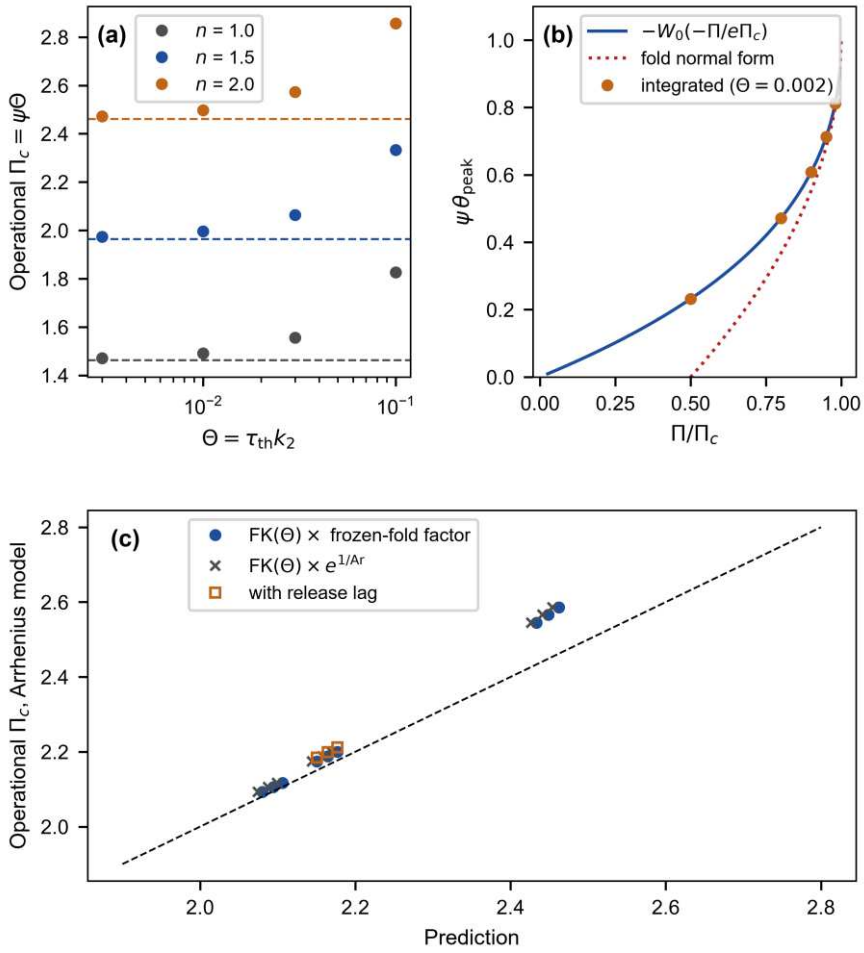


Fig. 3 (a) Operational critical number against Θ for n = 1, 3/2 and 2 (points: numerical integrations, not joined by a line; dashed: finite-ε Eq. (14)). (b) Quasi-steady overshoot below Π_c: Lambert-W formula, fold normal form, and integrations. (c) Arrhenius operational critical number against FK(Θ) times the frozen-fold factor. All points are results of numerical integration of the model equations; no experimental data are shown

3.5 Proposition 5: continuous-flow reactor, steady states, stability, and hysteresis

Let fresh resin of conversion 0 enter at the wall temperature with residence time τ_{res}, and let $\vartheta = \tau_{th}/\tau_{res}$ and $D = k_2\tau_{res}$. In units of τ_{res} and in the exponential model,

$$\frac{d\alpha}{dt'} = Dr - \alpha, \quad \frac{d\theta}{dt'} = Dr - \theta\left(1 + \frac{1}{\vartheta}\right), \quad r = (\varepsilon + \alpha)(1-\alpha)^n e^{\psi\theta}. \tag{16}$$

Control parameter. In the exponential model D is varied at fixed ϑ and ψ. This is a mathematical parameter sweep, not by itself a physical temperature sweep: a change of the wall temperature also changes $\psi = \Delta T_{ad}E_2/(RT_\infty^2)$, $\varepsilon = k_1/k_2$ and Ar. The ln D windows below are therefore windows in the parameter D, and no conversion of ln D into kelvin is claimed from them. A physical temperature path with Arrhenius kinetics, in which ψ, ε and D all change with T_∞, is simulated separately at the end of this section. A sweep of the flow rate at fixed temperature changes τ_{res} and therefore ϑ, which is a different parameter path and is not analyzed here.

Proposition 5 (steady states). The steady states satisfy $\theta = \vartheta\alpha/(1 + \vartheta) = \kappa\alpha/\psi$ and are given parametrically by

$$D = \frac{\alpha}{(\varepsilon + \alpha)(1 - \alpha)^n \exp(\kappa\alpha)}, \quad \kappa = \frac{\psi\vartheta}{1 + \vartheta}. \tag{17}$$

Proof. At steady state the conversion balance gives rD = α, and the heat balance gives $\theta(1 + 1/\vartheta)$ = rD = α, so $\theta = \vartheta\alpha/(1 + \vartheta) = \kappa\alpha/\psi$; substituting $\psi\theta = \kappa\alpha$ into rD = α gives the expression. ■ $D(\alpha)$ is non-monotonic, so three steady states coexist in a window of D, if and only if $d \ln D/d\alpha = 0$ has two roots, $n/(1 - \alpha) + \varepsilon/[\alpha(\varepsilon + \alpha)] = \kappa$. The left side has a single minimum, so three equilibria exist if and only if $\kappa > \kappa_c = \min_\alpha[n/(1 - \alpha) + \varepsilon/(\alpha(\varepsilon + \alpha))]$ ($\kappa_c = 1.894$ for $n = 3/2$ and $\varepsilon = 3 \times 10^{-3}$; $\kappa_c \to n$ as $\varepsilon \to 0$). Equilibrium multiplicity does not by itself establish two stable states or switching at both folds.

Stability. Let $q = \alpha/(\varepsilon + \alpha) - n\alpha/(1 - \alpha)$. Differentiating Eq. (16) at a steady state, with D and ϑ fixed, gives the Jacobian in the variables (α, θ)

$$J = [[\, q - 1\,,\ \psi\alpha\,]\,,[\, q\,,\ \psi\alpha - 1 - 1/\vartheta\,]] \tag{18}$$

with trace $q + \psi\alpha - 2 - 1/\vartheta$ and determinant $(1 + 1/\vartheta)(1 - q) - \psi\alpha$. At a fold the determinant vanishes and the other eigenvalue equals the trace. The lower fold has a negative trace for all cases below, so it is a saddle-node at which the lower (unreacted) state disappears. The upper fold has a negative trace, and is a saddle-node at which a stable upper state disappears, only for ψ below about 7.01 ($\vartheta = 1$); above it the trace at the upper fold is positive (+6.50 for $\psi = 20$: $\alpha = 0.8499$, ln D = -5.658), so the upper branch near its fold is unstable and becomes stable only above a larger conversion α_H at which the trace vanishes ($\alpha_H = 0.9158$, ln D_H = -5.450 for $\psi = 20$, with determinant 14.3 > 0, a Hopf-type point). The window of two stable states is therefore (ln D_{ext}, ln D_{ign}), where ln D_{ign} is the lower (ignition) fold and ln D_{ext} is the upper fold when its trace is negative and ln D_H otherwise (Table 7).

Table 7 Steady states and stability of the continuous-flow reactor ($\vartheta = 1$, $n = 3/2$, $\varepsilon = 3 \times 10^{-3}$, $\kappa_c = 1.894$). The upper branch is stable from the upper fold ('fold') or from the Hopf-type point ('hopf'); the attractor loop area is $\int(\alpha_{upper} - \alpha_{lower})\, d \ln D$ over the window of two stable states, and the fold-to-fold area uses the full multiplicity interval.

ψ	κ	Equilibria	Trace at upper fold	Upper stable from	ln D window of two stable states	Attractor loop area	Fold-to-fold area
3.0	1.50	1 ($\kappa < \kappa_c$)	–	–	–	0	0
4.5	2.25	3	-1.27	fold, $\alpha = 0.325$	-0.151 to -0.091	0.025	0.025
6.0	3.00	3	-0.51	fold, $\alpha = 0.498$	-0.466 to -0.130	0.227	0.227
8.0	4.00	3	+0.50	hopf, $\alpha = 0.710$	-0.987 to -0.169	0.678	0.710
12.0	6.00	3	+2.50	hopf, $\alpha = 0.844$	-2.280 to -0.225	1.921	2.040
20.0	10.00	3	+6.50	hopf, $\alpha = 0.916$	-5.450 to -0.307	5.047	5.236

Verification by attractors. We integrated Eq. (16) at fixed D from the unreacted state, from a mid-conversion state and from small perturbations of the upper steady state, for nine values of ln D around each window (ψ = 4.5 and 20). Two distinct long-time states were found for exactly those values of ln D that lie inside the window of Table 7 (ψ = 4.5: 3 of 3 inside values show two attractors; ψ = 20: 5 of 5), one state outside it, and no sustained oscillation anywhere (largest late-time oscillation amplitude in α: 2.8e-16). At ψ = 20 the perturbed upper state collapses to the lower state for ln D just below ln D_H, so the loss of stability at the Hopf-type point is, in these simulations, abrupt (subcritical-like), not a transition to a stable cycle; the unstable cycle, if any, was not computed.

The Hopf-type point (ψ = 20). At α_H = 0.9158 (ln D_H = -5.450) the Jacobian has a purely imaginary pair $\pm i\omega$ with ω = 3.784 (period 1.66 residence times) and determinant 14.3 > 0; the real part of the pair has nonzero speed, d$\mathrm{Re}\,\lambda/d$ ln D = -12.25 (transversality), so the eigenvalues cross the imaginary axis. Along the upper branch the eigenvalues are real at the fold (0 and 6.50), an unstable node, then an unstable focus, then a stable focus above ln D_H and a stable node far above. Whether the bifurcation is sub- or supercritical was probed numerically by the radius of the basin of the upper state: the smallest perturbation in θ that sends the trajectory to the lower state is 0.0045 at ln D = ln D_H + 0.01 and varies as the distance from the Hopf-type point to the power 0.57 (prefactor 0.045), so an unstable cycle that shrinks onto the equilibrium at ln D_H is indicated, i.e. a subcritical bifurcation. This is numerical evidence, not a proof: the first Lyapunov coefficient and the cycle itself were not computed.

Sweeps. We swept ln D up and down at rates v = 0.02, 0.01, 0.005, 0.002, 0.001, 0.0005 and 0.0002 per residence time (protocol in Appendix A: start at the unreacted state, dwell 20 residence times at each turning point, sweep bounds ±2 in ln D beyond the window). For ψ = 4.5, where the upper fold is a saddle-node, the sweep area decreases toward the attractor loop area (0.025; integrated 0.037 at v = 0.0002; fit A_0 = 0.025, p = 0.63). For ψ = 3 (κ = 1.50 < κ_c) there is no static loop and the area at v = 0.0002 is 0.002. A finite-rate loop exists below the threshold as well, so only convergence with v distinguishes a static loop from a rate-dependent one (Table 8). **For ψ = 8 and 20, where the upper branch loses stability at the Hopf-type point, convergence of the sweep area to the attractor loop area is not confirmed.** For ψ = 20 the integrated area falls from 5.427 to 5.144 over the rates and a power-law fit $A(v) = A_0 + cv^p$ gives A_0 = 5.119 (p = 0.62), above the attractor loop area 5.047; for ψ = 8 the attractor loop area is 0.678, the integrated area at v = 0.0002 is 0.722 and the fit gives 0.706.

Why the Hopf-type case is not simply a slow limit. The downward switching of the sweeps at ψ = 20 occurs between the Hopf-type point (ln D = -5.45) and the upper fold (-5.66), where the unstable upper equilibrium still exists. In a noise-free system a trajectory that follows the stable branch would stay on the unstable equilibrium until it disappears at the fold, and the loop would extend to the fold-to-fold area (5.236); in a real or numerical system, perturbations of size set by the noise grow and the exit occurs earlier. The simulations show exactly this dependence: at v = 0.001 the switching value of ln D is -5.575, -5.533, -5.502 and -5.508 for integrator tolerances (rtol) of 10^{-6}, 10^{-8}, 10^{-10} and 10^{-12}, with areas 5.200, 5.162, 5.134 and 5.140, while it does not depend on the turning point of the sweep (ln D_{ign} + 0.5 to + 3: -5.539 to -5.533). At the slower rates ($v \leq 0.002$) the sweep loop through a Hopf-type point lies between the attractor loop area (5.047) and the fold-to-fold area (5.236), and its limit at

vanishing sweep rate depends on the noise level; whether it tends to the attractor loop area as the noise-limited exit approaches the Hopf-type point requires a slow-passage analysis that is not attempted here.

Table 8 Integrated hysteresis-loop area $\oint \alpha \, d \ln D$ of the sweeps at seven sweep rates v (per residence time), with the attractor loop area, the fold-to-fold multiplicity area and a power-law fit $A(v) = A_0 + cv^p$ ($\vartheta = 1$, $n = 3/2$, $\varepsilon = 3 \times 10^{-3}$).

ψ	κ	Attractor loop area	Fold-to-fold area	$v = 0.02$	0.01	0.005	0.002	0.001	0.0005	0.0002	Fit A_0 (p)
3.0	1.50	0.000	0.000	0.125	0.069	0.037	0.016	0.008	0.004	0.002	-0.001 (0.86)
4.5	2.25	0.025	0.025	0.248	0.170	0.118	0.077	0.059	0.047	0.037	0.025 (0.63)
8.0	4.00	0.678	0.710	0.976	0.884	0.823	0.773	0.751	0.736	0.722	0.706 (0.60)
20.0	10.00	5.047	5.236	5.427	5.340	5.246	5.186	5.168	5.149	5.144	5.119 (0.62)

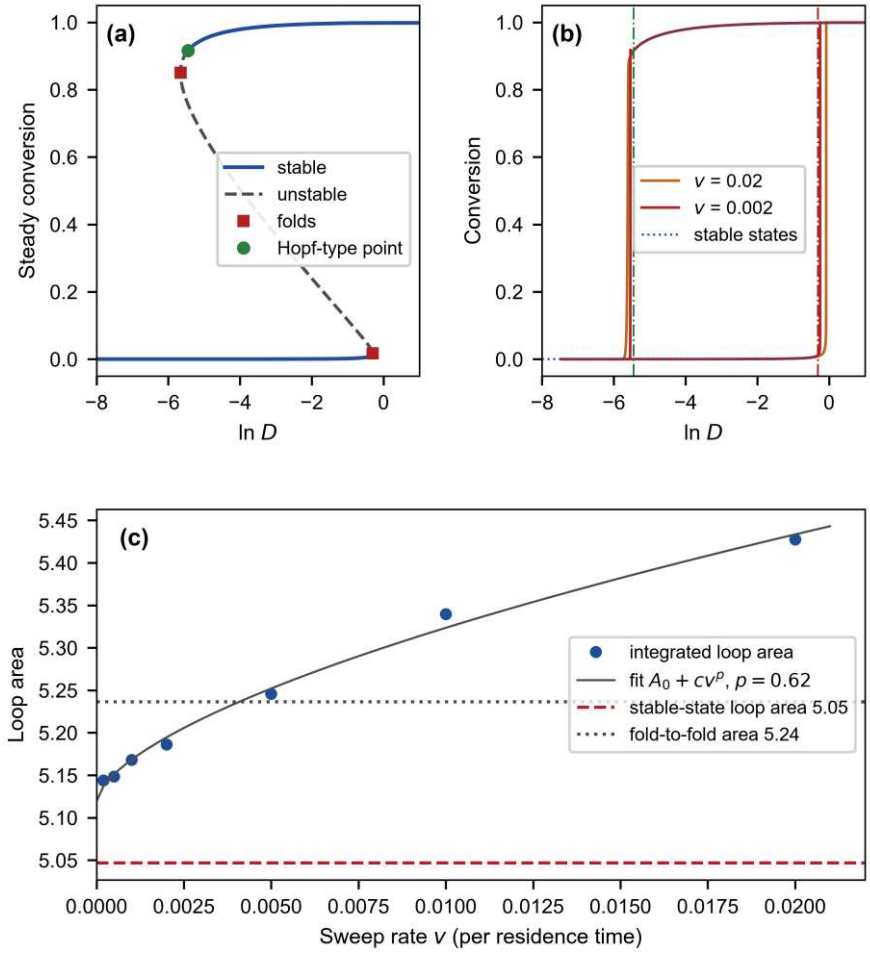


Fig. 4 (a) Steady-state curve of the flow reactor at $\psi = 20$ ($\kappa = 10$) with stable (solid) and unstable (dashed) segments, the two folds (squares) and the Hopf-type point (circle). (b) Sweep loops at two rates against the steady states. (c) Loop area from numerical integration (points, not joined by a line) against sweep rate, the power-law fit (line), and the attractor loop area (dashed)

Physical temperature path with Arrhenius kinetics. To avoid the fixed-ψ approximation, the continuous-flow reactor was also simulated with both $k_1(T)$ and $k_2(T)$ Arrhenius (Table 2), $\tau_{res} = \tau_{th} = 3$ min ($\vartheta = 1$), $n = 3/2$ and a wall temperature T_∞ that is varied, so that ψ, ε and D change along the path. The steady states are obtained exactly

(conversion balance solved for T at given α, $T_\infty = T - \Delta T_{ad}\vartheta\alpha/(1+\vartheta)$) and their stability from the numerical Jacobian (Table 9). For ΔT_{ad} = 220 K the ignition fold is at T_∞ = 152.09 °C and the upper branch is stable from T_∞ = 127.89 °C (a Hopf-type point, 0.74 K above the upper fold at 127.15 °C), giving a window of two stable states of 24.2 K; the local ψ is 9.3 at the ignition fold and 7.9 at the upper fold. For ΔT_{ad} = 160 K the window is 9.4 K (upper fold stable) and for 120 K it is 2.1 K. The fixed-ψ exponential-model estimate evaluated with the local ψ and ε at the ignition fold gives 26.6, 11.2 and 2.7 K for ΔT_{ad} = 220, 160 and 120 K: of the right order but not equal to the simulated widths, which is why the physical path is simulated rather than inferred. Temperature ramps at 2, 0.5, 0.1, 0.02 K per residence time give loop areas $\oint\alpha\ \mathrm{d}T_\infty$ of 35.7, 26.4, 22.2, 20.8 K at ΔT_{ad} = 220 K, decreasing with the ramp rate; as in the exponential model, the approach to a static limit is slow and is not claimed.

Table 9 Window of two stable states on a physical temperature path with Arrhenius kinetics ($\tau_{res} = \tau_{th}$ = 3 min, n = 3/2): steady states exact, stability from the numerical Jacobian; the last column is the fixed-ψ exponential-model estimate at the local ψ and ε of the ignition fold, for comparison.

ΔT_{ad} (K)	T_∞ at ignition fold (°C)	ψ, ε at that fold	T_∞ at upper fold (°C)	Upper branch stable from (°C)	How	Window (K)	Fixed-ψ estimate (K)
120	154.70	5.02, 0.0052	152.61	152.61	fold	2.1	2.7
160	153.45	6.74, 0.0053	144.01	144.01	fold	9.4	11.2
220	152.09	9.32, 0.0053	127.15	127.89	hopf	24.2	26.6

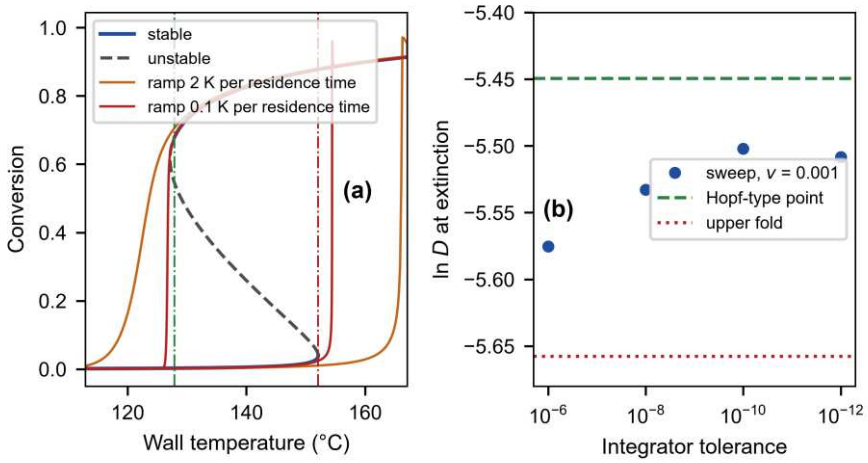


Fig. 5 (a) Steady states (solid: stable; dashed: unstable) and temperature ramps on the Arrhenius path (ΔT_{ad} = 220 K, $\tau_{res} = \tau_{th}$ = 3 min); the dash-dot lines mark the stable window. (b) Value of ln D at which the sweep of the exponential model (ψ = 20, ν = 0.001) leaves the upper branch, against the integrator tolerance (points: numerical integrations, not joined by a line), between the Hopf-type point and the upper fold

3.6 Closed forms as fitting functions: a synthetic-data test

With a known logistic width w_0, the storage curves depend on the capsule population only through the open fraction, i.e. through $z = (T_m - T_s)/\sigma_{eff}$ at each storage temperature, so the pair (T_m, σ) is determined only through the line $z(T_s) = (T_m - T_s)/\sigma_{eff}$; an unknown w_0 would add a third, confounded parameter. To see how well the pair can be recovered, synthetic isothermal storage curves were generated with the *population ODE* (not with the closed form) for σ = 5.0 °C, T_m = 118 °C and w_0 = 0.5 °C at three storage temperatures (112, 108, 105 °C) and five times (30–150

min), with Gaussian noise of 0.002 in conversion, and fitted by least squares with the closed form (known w_0; 200 noise realizations). The estimates are $\hat{\sigma} = 7.5 \pm 2.6$ °C and $\hat{T}_m = 120.9 \pm 3.1$ °C with a correlation of 0.97 (Fig. 6): the two parameters are almost degenerate in this design, and $\hat{\sigma}$ is biased high along the degenerate direction. An independent constraint on T_m, here a prior of 0.5 °C (as from a calorimetric endotherm), markedly improved recovery in this tested design, to $\hat{\sigma} = 5.1 \pm 0.4$ °C. Other temperatures, times or noise levels may also improve identifiability; no claim is made about real calorimetry.

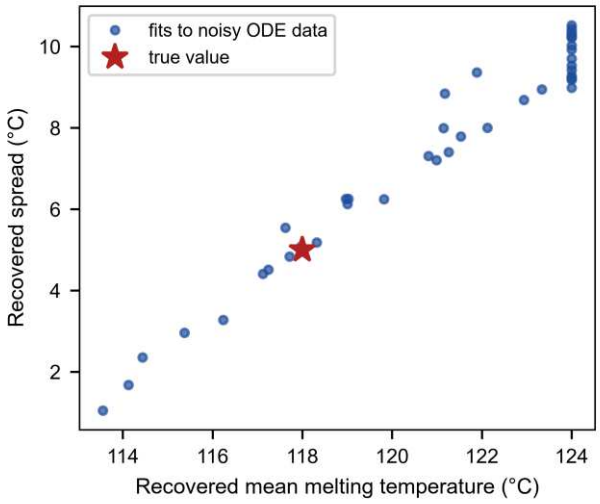


Fig. 6 Least-squares recovery of (T_m, σ) from noisy synthetic storage curves; each point is one noise realization (every fifth shown)

4 Status of the claims and approximations

Table 10 Status of the principal results, their assumptions, and where they fail or have not been tested. All parameters are illustrative.

Result	Status	Assumption it rests on	Where it fails or is untested
Availability clock (Prop. 1)	Exact	Constant temperature; $\alpha(0) = 0$, $C_i(0) = 0$; one availability function $\langle C \rangle(t)$	Temperature transients and exotherm; the delay is conversion dependent (Eq. (6)), and incomplete activation changes the clock
Isothermal time and sharpness (Prop. 2)	Exact (quadrature); $n = 1$ closed form; sharpness law asymptotic	$m = 1$; no diffusion control	Sharpness law only for $n = 1$ and $b \gg 9a$; vitrification not modelled
Storage conversion and σ^* (Prop. 3)	Linearized closed form; probit approximation; verified to a few percent	Gaussian spread; equal-mass independent capsules; small conversion	Large tolerance ($\eta \gtrsim 0.05$); skewed or bimodal distributions; capsule–capsule heat exchange
Critical number (Prop. 4)	Frozen-conversion fold, closed form; operational thresholds numerical	Exponential comparison model; ungated; $\Theta \to 0$	Finite Θ shifts Π_c upward (computed only); whether the fold marks ignition of a finite batch is numerical; spatial gradients absent
Arrhenius factor	Frozen-fold factor (exact for one Arrhenius source); $\exp(1/Ar)$ first-order	Single Arrhenius source for the fold	Tested only for $Ar = 18.0$–19.9 and $\Theta \leq 0.1$; not tested at small Ar
Flow reactor multiplicity (Prop. 5)	Exact for the stated model	Perfect mixing; exponential model; ungated; ϑ, ψ fixed	Real reactors: finite mixing time, wall–fluid temperature difference
Flow reactor stability	Jacobian exact; stable window computed; checked by simulation; Hopf character	As above	Hopf-type point studied for $\psi = 20$ only (subcritical bifurcation indicated numerically, no Lyapunov coefficient);

Result	Status	Assumption it rests on	Where it fails or is untested
	numerical		convergence of sweep loops to the attractor loop area unconfirmed (noise dependent)
Temperature path (Arrhenius)	Steady states exact; stability numerical	$\tau_{res} = \tau_{th} = 3$ min, $n = 3/2$, $\Delta T_{ad} = 120$, 160, 220 K	Other τ, ϑ, ΔT_{ad} not scanned; sweeps not converged
Parameter recovery (Section 3.6)	Numerical experiment	Gaussian noise; population ODE as truth; known w_0	Not a test on real calorimetry

Three approximations carry the paper: the lumped, well-mixed energy balance; the exponential linearization of the Arrhenius law near the fold; and the Gaussian, independent-capsule description of the population. The first is a deliberate scope limit and the second is quantified (Table 6); the third is tested only against population equations that use the same description.

5 Falsifiable signatures

Each proposition predicts a measurement that a standard calorimetric or rheological experiment can make; none has been made here. (1) *Availability clock.* Isothermal DSC at several temperatures above the melting endotherm, comparing the gated resin with the same resin with the catalyst dissolved, should give a delay that depends on conversion as Eq. (6) and approaches $\tau_{rel}(T)$ at late conversion; a conversion-dependent delay does not falsify the single-availability-function description, which predicts it. What would falsify it is a failure of the measured gated curves, replotted on the integrated-availability clock (measured independently, for example by release assays), to collapse onto the ungated curve. (2) *Storage bound.* The melting endotherm gives T_m and σ; isothermal storage at a margin Δ for a time t should then give a conversion within a few tens of percent of Eq. (11); a systematically larger conversion would indicate a tail of capsules with low melting temperature that the Gaussian description misses. (3) *Critical thermal time constant.* At fixed T_∞, specimens of increasing thickness (τ_{th} grows as thickness squared) should show a rapid rise of the peak temperature rise at an operational threshold near $\Pi_c/(\psi k_2)$, with the Arrhenius factor of Eq. (15); the abruptness of the rise, from $O(\Theta)$ to $O(\Delta T_{ad})$, is the signature of the fold. (4) *Window of two stable states.* In a continuously fed reactor with flow rate and wall time constant held fixed, a slow ramp of the wall temperature up and down should show an ignition at the temperature of the lower fold and an extinction at a lower temperature, with a window of the width computed for the actual (Arrhenius) path (Table 9; 24 K for the illustrative $\Delta T_{ad} = 220$ K). The loop must be examined as the ramp slows; a loop that closes is rate dependent and not bistability. Where the upper state is lost at a Hopf-type point the extinction temperature is expected to lie between the Hopf-type point and the upper fold and to depend on the noise level of the experiment, so a single extinction temperature should not be predicted there. A sweep of the flow rate at fixed temperature is a different path (ϑ changes) and is not covered by the analysis.

6 Open problems

(a) *Spatial extension.* The lumped balance replaces the classical slab, cylinder or sphere. The critical Frank-Kamenetskii parameter of a consuming, autocatalytic source in a spatially resolved specimen, and its relation to Π_c above, are open. (b) *Finite-Θ correction.* The upward shift of Π_c with Θ is computed numerically; a closed-form

first correction would complete Proposition 4. (c) *Hopf-type point and slow passage.* The first Lyapunov coefficient, the unstable cycle, and an analysis of the slow passage (noise-limited delay) that would predict the limit of the sweep loops were not attempted; the sub- or supercritical character was probed only for $\psi = 20$. (d) *Non-Gaussian populations.* Proposition 3 needs only the lower tail of the melting-temperature distribution; skewed and bimodal distributions, and capsule–capsule heat exchange, are untested. (e) *Diffusion control and vitrification.* These stop the cure before completion and change the late-time tail of Proposition 2. (f) *Noise.* In small specimens or flow channels the fold may be crossed by fluctuations. (g) *Gated thermal and flow analysis.* The criticality and reactor analyses of Propositions 4 and 5 use a fully released catalyst; the combined effect of a partly open, slowly releasing population and thermal feedback is not analyzed here; it is the setting of the earlier numerical study [18]. (h) *Experiment.* The propositions are untested on a real encapsulated system; the signatures of Section 5 are the proposed tests.

7 Conclusion

For the lumped model of a melt-gated autocatalytic cure, several statements can be made exactly or in closed form. The gated cure at constant temperature is the isothermal cure on the clock of integrated availability, and the delay of a fully open population is $\tau_{rel}[1 - \exp(-t/\tau_{rel})]$ (Proposition 1). The isothermal cure time is exact by quadrature, and the $n = 1$ sharpness is a logarithm of the rate-constant ratio (Proposition 2). The storage conversion of a Gaussian capsule population is $(a/b)[\exp(b\ f\ t_{eff}) - 1]$, which inverts into a bound on the melting-temperature spread (Proposition 3). For a fully released catalyst, the frozen-conversion thermal balance has a critical number $(1+n)^{1+n}/[e\ n^n(1+\varepsilon)^{1+n}]$, with an Arrhenius correction that is close to $\exp(1/Ar)$ in the tested grid (Proposition 4). The continuous-flow reactor (ungated kinetics) has three equilibria above κ_c, but the upper branch can lose stability at a Hopf-type point before its fold, so the hysteresis window and its loop area must be computed from the stable states, and sweep loops through that point depend on noise (Proposition 5). Propositions 4 and 5 are derived for a fully released catalyst; their extension to the gated reactor, in which release and melting add further time scales, is not derived here. All results are tested against the full equations; none is tested against experiment, and the parameters are illustrative.

Statements and Declarations

Funding. No funds, grants, or other support was received.

Competing interests. The author has no relevant financial or non-financial interests to disclose.

Author contributions. Conceptualization: Leon Sandler; Methodology: Leon Sandler; Software: Leon Sandler; Formal analysis and investigation: Leon Sandler; Writing – original draft preparation: Leon Sandler; Writing – review and editing: Leon Sandler; Visualization: Leon Sandler.

Ethics approval. Not applicable.

Related work. A related numerical study by the author [18, 19] is posted as a preprint and has been submitted elsewhere; the relationship is described in Section 1.1.

Use of artificial intelligence. Claude Sonnet 5.5 (Anthropic) was used for derivations, code, figures and drafting as described in Section 2.3; the author is responsible for the content.

Data and code availability. The model code, the closed-form module, the tests, the figure scripts, the results file (results.json) and the manuscript builder are available at https://github.com/sandlerleon/gated-autocatalysis-criticality (release *v*1.3.2) and archived on Zenodo at https://doi.org/10.5281/zenodo.23306493; this manuscript is archived as a preprint at https://doi.org/10.5281/zenodo.23306494.

Appendix A. Numerical protocol, tolerances and convergence

Reference integrator. Eqs. (1)–(3) are integrated for all scenarios at once with a vectorized fixed-step fourth-order Runge–Kutta scheme (step 0.01 min for Sections 3.1 and 3.2, 0.05 min for the population runs of Section 3.3; end time 150 min for storage, 300–600 min for cure times). Conversion is limited to [0, 1] and the reaction heat is $\Delta T_{ad}\, d\alpha/\mathrm{dt}$ without cut-off, so the energy balance is conserved: in the adiabatic limit the integrated temperature rise equals $\Delta T_{ad}\alpha$ to 6.2e-08 K (Section 2, test_theory.py). Capsule populations use K deterministic Gaussian quantiles $z_i = \Phi^{-1}[(i - 1/2)/K]$: $K = 3201$ for the storage-conversion and design-rule comparisons of Section 3.3, and $K = 801$ for the step study and the recovery test. Convergence is reported separately for the two sources of numerical error, so that neither is mistaken for error of the closed forms. Population discretization: relative to $K = 6401$ the storage conversion differs by at most 1.1e-02 at $K = 801$ (the narrow spread $\sigma = 2$ °C is the tail-sensitive case) and by at most 4.9e-04 at $K = 3201$. Time step: relative to step 0.0125 min the step 0.05 min differs by at most 3.1e-14 (Table 11; difference = value/reference − 1). The deviations of Section 3.3 are therefore dominated by the approximations of the closed forms, not by the reference calculation.

Adaptive integrations. The exponential-model criticality problem is integrated with LSODA (an adaptive stiff/non-stiff ODE solver; relative tolerance rtol 10^{-9}, absolute tolerance atol 10^{-13}, max step 0.02, end time $40/k_2$); the Arrhenius criticality problem with LSODA (rtol 10^{-8}, atol 10^{-12}, end time $60/k_2$, temperature floored at 200 K in the rate); the flow reactor with LSODA (rtol 10^{-8}, atol 10^{-12}, max step $\min(0.5, 0.02/v)$); fixed-D attractor runs with LSODA (rtol 10^{-11}, atol 10^{-14}, end time 3000 residence times; the last 10 % is used to classify the state); constant-temperature delay checks with RK45 (rtol 10^{-12}).

Noise and temperature-path studies. The tolerance study uses LSODA with (rtol, atol) = (10^{-6}, 10^{-9}), (10^{-8}, 10^{-12}), (10^{-10}, 10^{-14}) and (10^{-12}, 10^{-16}) at $v = 0.001$; the basin radius is bisected (26 steps, bracket [10^{-6}, 0.5]) in the direction of $-\theta$ with end time 2500 residence times. The Arrhenius temperature path uses 4000 conversion points for the steady curve (brentq xtol 10^{-10} in T), a central-difference Jacobian, and LSODA ramps (rtol 10^{-8}, atol 10^{-10}, dwell 20 residence times, bounds from 15 K below the window to 15 K above it). *Thresholds.* The operational critical number is the Π (exponential model, bracket [0.3, 8], 30 bisection steps) or the adiabatic rise (Arrhenius model, bracket [3, 8000] K in logarithm, 26 steps) at which the integrated peak temperature rise $(T_{max} - T_\infty)/\Delta T_{ad}$ first exceeds 0.3, starting from $T(0) = T_\infty$. *Sweeps.* Start at $(\theta, \alpha) = (0, 0)$ at the lower bound of ln D (window lower edge minus 2), dwell 20 residence times, sweep up at rate v to the upper bound (window upper edge plus 2), dwell 20, sweep down, dwell 20; the area is the signed integral of $\alpha\, d\ln D$ over the two sweep legs (output step 0.05).

Design bound. σ^* from Eq. (12) with w_0 = 0.5 °C; the ODE root is bracketed in [0.3, 40] °C (xtol 10^{-3}). *Recovery.* 200 noise realizations (seed 20261007, prior test seed 20261008), bounded least squares. *Errors.* In every table, difference = closed form (or prediction)/numerical − 1. *Software.* Python 3.11.9, NumPy 2.4.6, SciPy 1.17.1; release *v*1.3.2 of the repository contains the exact scripts and results.json.

Table 11 Convergence of the reference integrator with population size and step (storage conversion after 150 min, Δ = 6 °C, w_0 = 0.5 °C; the narrower spread σ = 2 °C is the tail-sensitive case; the step study uses K = 801).

Quantity	Setting	Value at setting	Reference	Relative difference
Storage conversion (σ = 2 °C, Δ = 6 °C)	K = 101	0.000101	0.000142 (K = 6401)	-2.9e-01
Storage conversion (σ = 2 °C, Δ = 6 °C)	K = 201	0.000124	0.000142 (K = 6401)	-1.3e-01
Storage conversion (σ = 2 °C, Δ = 6 °C)	K = 401	0.000136	0.000142 (K = 6401)	-4.2e-02
Storage conversion (σ = 2 °C, Δ = 6 °C)	K = 801	0.000140	0.000142 (K = 6401)	-1.1e-02
Storage conversion (σ = 2 °C, Δ = 6 °C)	K = 1601	0.000142	0.000142 (K = 6401)	-2.5e-03
Storage conversion (σ = 2 °C, Δ = 6 °C)	K = 3201	0.000142	0.000142 (K = 6401)	-4.9e-04
Storage conversion (σ = 2 °C, Δ = 6 °C)	step 0.2 min	0.000140	0.000140 (step 0.0125)	+6.7e-15
Storage conversion (σ = 2 °C, Δ = 6 °C)	step 0.1 min	0.000140	0.000140 (step 0.0125)	-1.6e-14
Storage conversion (σ = 2 °C, Δ = 6 °C)	step 0.05 min	0.000140	0.000140 (step 0.0125)	-3.1e-14
Storage conversion (σ = 2 °C, Δ = 6 °C)	step 0.025 min	0.000140	0.000140 (step 0.0125)	-3.7e-14
Storage conversion (σ = 2 °C, Δ = 6 °C)	step 0.0125 min	0.000140	0.000140 (step 0.0125)	+0.0e+00
Storage conversion (σ = 4 °C, Δ = 6 °C)	K = 101	0.003681	0.003681 (K = 6401)	+1.0e-06
Storage conversion (σ = 4 °C, Δ = 6 °C)	K = 201	0.003681	0.003681 (K = 6401)	+7.4e-08
Storage conversion (σ = 4 °C, Δ = 6 °C)	K = 401	0.003681	0.003681 (K = 6401)	+5.3e-09
Storage conversion (σ = 4 °C, Δ = 6 °C)	K = 801	0.003681	0.003681 (K = 6401)	+3.7e-10
Storage conversion (σ = 4 °C, Δ = 6 °C)	K = 1601	0.003681	0.003681 (K = 6401)	+2.4e-11
Storage conversion (σ = 4 °C, Δ = 6 °C)	K = 3201	0.003681	0.003681 (K = 6401)	+1.1e-12
Storage conversion (σ = 4 °C, Δ = 6 °C)	step 0.2 min	0.003681	0.003681 (step 0.0125)	-8.2e-13
Storage conversion (σ = 4 °C, Δ = 6 °C)	step 0.1 min	0.003681	0.003681 (step 0.0125)	-4.9e-14
Storage conversion (σ = 4 °C, Δ = 6 °C)	step 0.05 min	0.003681	0.003681 (step 0.0125)	-2.2e-16
Storage conversion (σ = 4 °C, Δ = 6 °C)	step 0.025 min	0.003681	0.003681 (step 0.0125)	+4.4e-16
Storage conversion (σ = 4 °C, Δ = 6 °C)	step 0.0125 min	0.003681	0.003681 (step 0.0125)	+0.0e+00

Table 12 Run table of the numerical studies; every result is reproduced by code/run_all.py.

Study	Method	Grid	Compared with
Availability clock	RK4 (step 0.01 min) and RK45 (rtol 10^{-12}), constant T	T = 125, 140, 155 °C; α = 0.001–0.9	Eqs. (5), (6)
Isothermal cure	RK4, step 0.01 min	T = 110–155 °C; n = 1, 3/2	Quadrature; Eqs. (7), (8), (9)
Storage conversion	RK4 population (K = 3201), step 0.05 min	Δ = 3, 6, 10 °C; σ = 2–10 °C; t = 150 min	Eq. (11)
Design bound	Root-finding on the population ODE	Δ = 3, 6, 10 °C; η = 0.001, 0.01, 0.05	Eq. (12)
Criticality (exponential model)	LSODA, bisection	n = 1, 3/2, 2; Θ = 0.1–0.003	Eq. (14)
Criticality (Arrhenius)	LSODA, bisection	T = 120, 140, 160 °C; Θ = 0.01–0.1	Eq. (15)
Flow reactor	Jacobian; LSODA attractors and sweeps	ψ = 3, 4.5, 6, 8, 12, 20; ν = 0.02–0.0002	Eqs. (17), (18), attractor loop area
Hopf-type point and noise	Eigenvalues, basin radius, tolerance study	ψ = 20; ln D_H + 0.01 to + 0.95; rtol 10^{-6}–10^{-12}	Transversality, ω, attractor and fold-to-fold areas
Arrhenius temperature path	Exact steady states, Jacobian, LSODA ramps	ΔT_{ad} = 120, 160, 220 K; ramps 2–0.02 K per τ_{res}	Table 9
Parameter recovery	Bounded least squares, 200 noise draws	3 temperatures × 5 times	Truth

References

1. White SR, Sottos NR, Geubelle PH, Moore JS, Kessler MR, Sriram SR, et al (2001) Autonomic healing of polymer composites. Nature 409:794-797. https://doi.org/10.1038/35057232

2. Jamekhorshid A, Sadrameli SM, Farid M (2014) A review of microencapsulation methods of phase change materials (PCMs) as a thermal energy storage (TES) medium. Renewable and Sustainable Energy Reviews 31:531-542. https://doi.org/10.1016/j.rser.2013.12.033

3. Siepmann J, Siepmann F (2012) Modeling of diffusion controlled drug delivery. Journal of Controlled Release 161:351-362. https://doi.org/10.1016/j.jconrel.2011.10.006

4. Kamal MR, Sourour S (1973) Kinetics and thermal characterization of thermoset cure. Polymer Engineering & Sci 13:59-64. https://doi.org/10.1002/pen.760130110

5. Sourour S, Kamal MR (1976) Differential scanning calorimetry of epoxy cure: isothermal cure kinetics. Thermochimica Acta 14:41-59. https://doi.org/10.1016/0040-6031(76)80056-1

6. Bogetti TA, Gillespie JW (1992) Process-Induced Stress and Deformation in Thick-Section Thermoset Composite Laminates. Journal of Composite Materials 26:626-660. https://doi.org/10.1177/002199839202600502

7. Semenoff N (1928) Zur Theorie des Verbrennungsprozesses. Z Physik 48:571-582. https://doi.org/10.1007/bf01340021

8. Frank-Kamenetskii DA (1969) Diffusion and heat transfer in chemical kinetics, 2nd edn. Plenum Press, New York

9. Adler J, Enig JW (1964) The critical conditions in thermal explosion theory with reactant consumption. Combustion and Flame 8:97-103. https://doi.org/10.1016/0010-2180(64)90035-5

10. Kassoy DR, Poland J (1980) The Thermal Explosion Confined by a Constant Temperature Boundary:I—The Induction Period Solution. SIAM J Appl Math 39:412-430. https://doi.org/10.1137/0139035

11. van Heerden C (1953) Autothermic Processes. Ind Eng Chem 45:1242-1247. https://doi.org/10.1021/ie50522a030

12. Aris R, Amundson NR (1958) An analysis of chemical reactor stability and control—I. Chemical Engineering Science 7:121-131. https://doi.org/10.1016/0009-2509(58)80019-6

13. Uppal A, Ray WH, Poore AB (1974) On the dynamic behavior of continuous stirred tank reactors. Chemical Engineering Science 29:967-985. https://doi.org/10.1016/0009-2509(74)80089-8

14. Gray P, Scott SK (1990) Chemical oscillations and instabilities: non-linear chemical kinetics. Clarendon Press, Oxford

15. Vyazovkin S, Burnham AK, Criado JM, Pérez-Maqueda LA, Popescu C, Sbirrazzuoli N (2011) ICTAC Kinetics Committee recommendations for performing kinetic computations on thermal analysis data. Thermochimica Acta 520:1-19. https://doi.org/10.1016/j.tca.2011.03.034

16. Zhao Y, Drummer D (2019) Influence of Filler Content and Filler Size on the Curing Kinetics of an Epoxy Resin. Polymers 11:1797. https://doi.org/10.3390/polym11111797

17. Ozawa T (1965) A New Method of Analyzing Thermogravimetric Data. Bulletin of the Chemical Society of Japan 38:1881-1886. https://doi.org/10.1246/bcsj.38.1881

18. Sandler L (2026) Coupled thermal activation and autocatalytic cure kinetics: a theoretical and computational study of delayed reactive transformation. ChemRxiv. https://doi.org/10.26434/chemrxiv.15008366/v1 (archived at https://doi.org/10.5281/zenodo.22073390)

19. Sandler L (2026) AutoLatch: coupled thermal activation and autocatalytic cure kinetics, version 3.1 (code and manuscript archive). Zenodo. https://doi.org/10.5281/zenodo.23202125

20. Strogatz SH (2015) Nonlinear dynamics and chaos, 2nd edn. Westview Press, Boulder

21. Corless RM, Gonnet GH, Hare DEG, Jeffrey DJ, Knuth DE (1996) On the LambertW function. Adv Comput Math 5:329-359. https://doi.org/10.1007/BF02124750